NANO LETTERS
Letter
Cite This: Nano Lett. 2019, 19, 9138–9144
pubs.acs.org/NanoLett

Mimicking Chemotactic Cell Migration with DNA Programmable Synthetic Vesicles

Jing Pan,[†] Yancheng Du,[†] Hengming Qiu, Luke R. Upton, Feiran Li, and Jong Hyun Choi*

School of Mechanical Engineering, Purdue University, West Lafayette, Indiana 47907, United States

Supporting Information

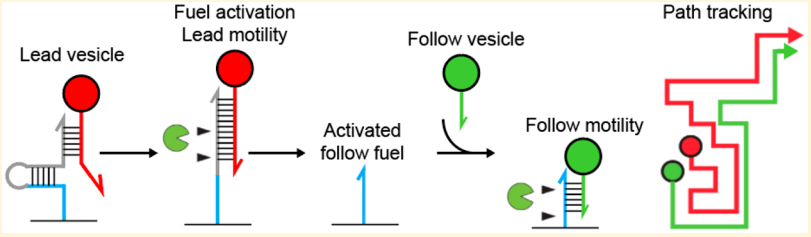

ABSTRACT: Chemotactic cell motility plays a critical role in many biological functions, such as immune response and embryogenesis. Constructing synthetic cell-mimicking systems, such as a dynamic protocell, likewise requires molecular mechanisms that respond to environmental stimuli and execute programmed motility behaviors. Although various molecular components were proposed to achieve diverse functions in synthetic protocells, chemotactic motility on surfaces has not been reported thus far. Here we show directional motility in synthetic lipid vesicles capable of chasing each other by programming DNA components. We demonstrate that the "follow" vesicle recognizes and migrates along the moving trajectory of the "lead" vesicle with an enhanced speed, thus mimicking natural chemotaxis in cell migration. This work provides new possibilities for building synthetic protocells with complex functions such as programmed morphogenesis and cooperative motion. With the vast library of dynamic DNA components, we envision that this platform will enable new discoveries in fundamental sciences and novel applications in biotechnology.

KEYWORDS: *Synthetic vesicles, protocells, DNA nanotechnology, DNA walker, chemotaxis, chemokinesis*

Downloaded via PURDUE UNIV on December 11, 2019 at 15:40:55 (UTC).
See https://pubs.acs.org/sharingguidelines for options on how to legitimately share published articles.

Cell motility is a crucial function that gives rise to various complex biological processes such as embryogenesis and wound repair.[1] Chemotactic cell migration on surfaces, in particular, plays a critical role in the immune response. For example, neutrophils chase bacteria by sensing biochemical signals and crawling with a sustained increase in speed (i.e., chemokinetic response) and ultimately engulf them via phagocytosis.[2,3] Recently, synthetic minimal cells were developed as a versatile platform for advancing fundamental understanding in biology[4] as well as for creating novel biomedical applications including drug delivery and chemical microreactors.[5,6] Engineering cell-mimicking functions such as directed motility in synthetic protocells will thus provide new opportunities. While various molecular machinery was developed to create biomimetic functions in synthetic protocells,[7,8] few mechanisms have been proposed for control of cell migration and chemotactic motility.[9]

Here we demonstrate dynamic synthetic vesicles (SVs) capable of chasing one another on two-dimensional (2D) surfaces by programming DNA components. As a programmable material, DNA has been engineered for generating synthetic molecular systems such as nanostructures,[10−12] affinity reagents,[13] motors,[14−16] and logic gates.[17,18] We show that directed motility in DNA functionalized SVs can be achieved by combining toehold switchable oligonucleotides with signaling strands and that the "follow" vesicle recognizes the path that the "lead" vesicle has traveled and tracks the trajectory with an enhanced speed. This work opens new possibilities for DNA programmable biochemical communication and coordination among protocells. The extensive library of dynamic DNA systems[10,19] may allow researchers to create complex behaviors in synthetic cells that could ultimately match the complexity of their natural counterparts.[8]

Natural cells and microorganisms such as *Rhodobacter sphaeroids* have two behavioral characteristics in chemotactic migration: (i) biochemical signal recognition and (ii) directed motility with an enhanced speed.[20] To engineer similar properties in protocells, we simplified our approach and designed two mechanisms based on phospholipid and nucleic acid chemistry. First, we self-assembled vesicles using phospholipid−oligonucleotide conjugates whose sequence contains our motility designs (see Supporting Information for sequence and method details). Figure 1a shows the scheme of the vesicle whose typical size is approximately 200 nm with DNA valency on the order of ∼500 strands per vesicle (Figures S1 and S2 and supplementary text). To achieve autonomous vesicle motility, we used DNA walkers, a type of dynamic DNA motif

Received: October 25, 2019
Revised: November 12, 2019
Published: November 15, 2019

© 2019 American Chemical Society

DOI: 10.1021/acs.nanolett.9b04428
Nano Lett. 2019, 19, 9138−9144

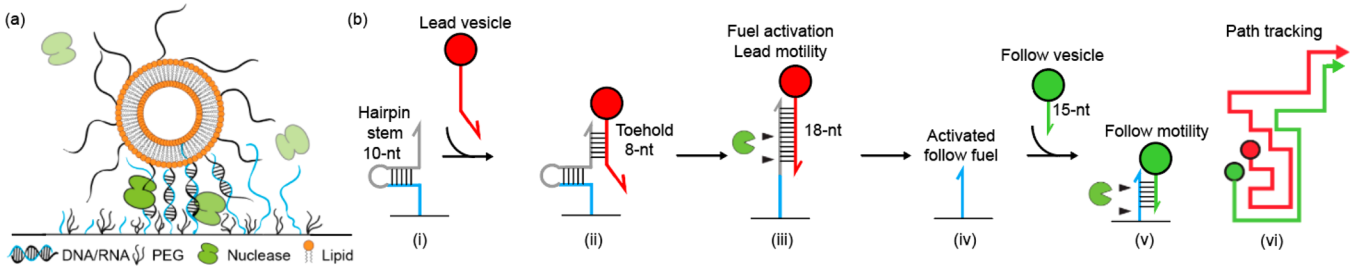

Figure 1. Synthetic vesicle (SV) with DNA programmable motility. (a) DNA (black) decorated on an SV (orange) hybridize with RNA (blue) fuels on a glass coverslip. Nuclease (green) cleaves the DNA/RNA duplex and moves the SV toward new, intact RNA fuels. Polyethylene glycol (PEG, black) is used to prevent undesired surface adsorption effects. (b) Scheme for synthetic chemotaxis. A "follow" vesicle (green) chases a "lead" vesicle (red), enabled by switchable RNA fuel, which contains two fuel domains (gray and blue) for lead and follow SVs. The follow SV fuel is initially shielded in a hairpin structure (i). A lead SV first associates with the lead fuel (gray) via 8-nt toehold (ii) and activates the fuel through strand displacement (iii). After the lead SV migrates toward adjacent unexplored fuel area (iv), the follow SV will then find the activated fuel (v) and experience a strong bias that forces it to move only along the trajectory of the lead SV, thus demonstrating the path tracking behavior (vi).

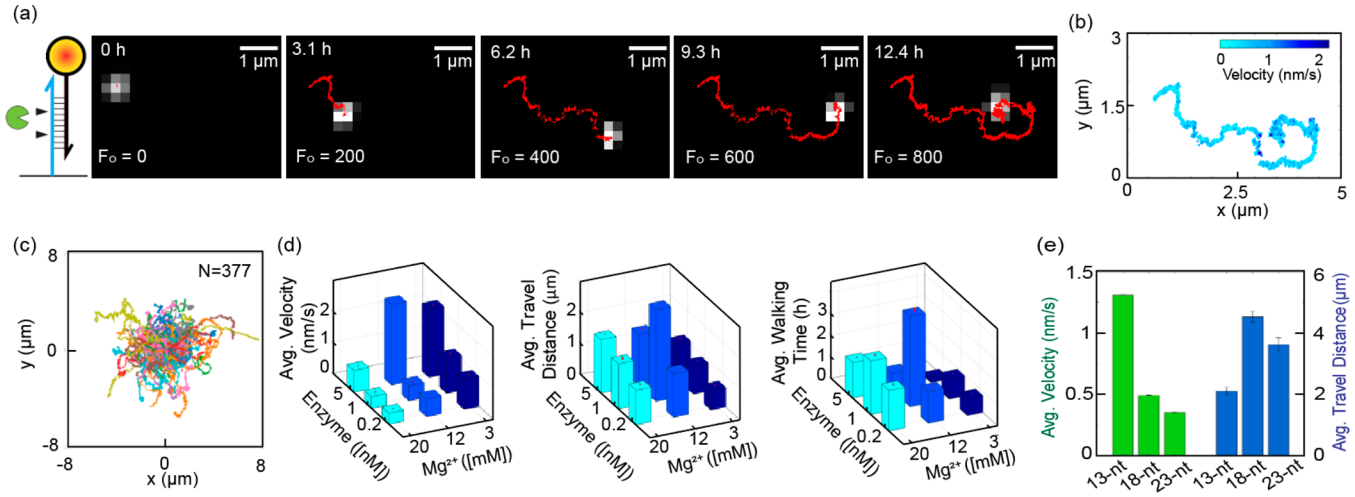

Figure 2. SV motility characterization. (a) Time-lapse images and trajectory (red) of a representative moving vesicle. The vesicle (orange) decorated with DNA (black) migrates on an RNA fuel (blue) surface. The experiment is performed in a buffer solution containing 12 mM Mg^{2+} and 1 nM nuclease. The time point of each image is shown in both time (hour) and dimensionless time, Fourier number ($Fo = Dt/r^2$ where D is the diffusion coefficient, t is time, and r is the radius of the vesicle). (b) Instantaneous velocity along the trajectory showing a consistent speed with an average of ~0.5 nm/s over a time period of more than 12 h. (c) Ensemble motility characteristics showing trajectories from moving SVs. (d) Effects of different experimental parameters, Mg^{2+} and nuclease concentrations, on velocity, distance, and travel time of SVs with 18-nt DNA. (e) Average velocity and distance for different DNA lengths.

that converts chemical energy into physical translocation, on an RNA "fuel" surface. The surface RNA density is characterized to have approximately 15 nm interstrand spacing on glass coverslips (Figures S3 and S4). Multiple mechanisms can be used to implement DNA powered walking reactions.[21,22] Here we adopted an endonuclease-driven "burnt-bridge" approach previously shown to move cargo randomly on surfaces.[23−25]

Next, we developed a mechanism for directed and chemokinetic motility using signaling oligonucleotides as illustrated in Figure 1b. The surface RNA consists of two fuel domains for lead (gray) and follow (blue) vesicles. The two fuels contain 10-nucleotide (nt) complementary segments and initially form a hairpin structure (state (i)). An 8-nt toehold is available for binding the lead SV (shown in red in Figure 1b, state (ii)). The hybridization of the lead SV activates the RNA switch through toehold-mediated strand displacement and exposes the follow fuel domain. After fuel activation, a nuclease will find and cleave the RNA fuel that the DNA on the vesicle binds with (state (iii)). Since the vesicle has multiple DNA/RNA duplexes, the enzymatic cleavage will drive the SV away from its current position rather than releasing it from the surface (state (iv)). Therefore, the vesicle will explore the fuel surface and migrate toward new unexplored regions with intact RNA fuels (i.e., self-avoiding motion). After lead SV movement, the follow vesicle (green) will hybridize to the now-activated fuel and start migration as shown in Figure 1b, state (v). The follow vesicle is designed with shorter DNA walkers than the lead vesicle so that the follow SV will chase the lead SV with an increased velocity on track. The most critical step in this process is that the follow vesicle will have a strong bias to stay on the activated fuels such that it will move only along the path that the lead SV has explored, thus chasing the lead vesicle (state (vi)).

To program SV motility, we first examined vesicle motion on straight fuels (Figure 2). We tracked the vesicle migration using time-lapse imaging and developed a quantitative understanding of the DNA powered SV motility. Previous studies demonstrated fluorescence-based single-particle tracking assays on DNA walkers and showed >1 nm/s in velocity and travel distance longer than 1 μm.[26−29] In this work, we imaged fluorophore-labeled DNA-vesicles with a custom-built total internal reflection fluorescence (TIRF) microscopy (Figure S6 and Movie S1).[30] The SVs are shown as a diffraction-limited

DOI: 10.1021/acs.nanolett.9b04428
Nano Lett. 2019, 19, 9138−9144

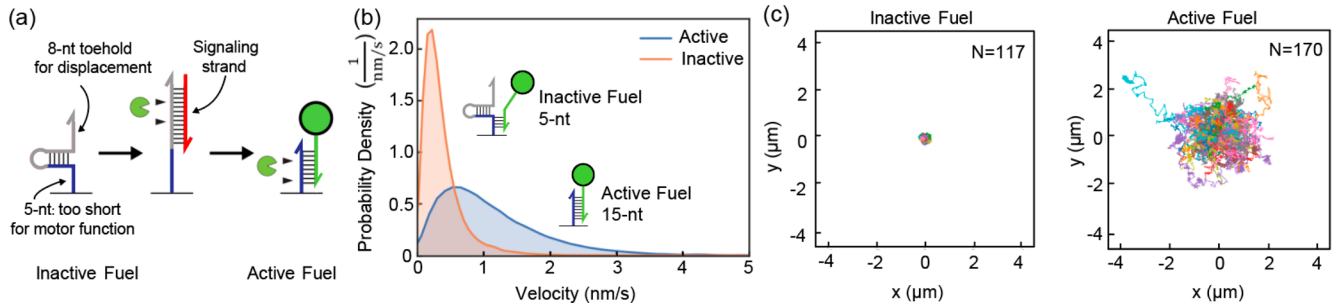

Figure 3. Motility control with a secondary structure of the fuel strand. (a) RNA fuel (dark blue) is shielded by an intramolecularly linked displacement strand (gray). Only a 5-nt toehold is available for binding with DNA strands on the vesicle. The displacement strand can be removed by a signaling oligonucleotide (red). Nuclease cleavage activates the fuel for the vesicle (green circle). (b) Velocity distributions of SVs on active (blue) and inactive (orange) fuels. (c) Trajectories of SVs on active (right) and inactive (left) fuels. All experiments were performed in a buffer with 3 mM Mg^{2+} and 1 nM enzyme.

spot in the image, and the subpixel positions are extracted by fitting a Gaussian distribution to the point spread function. A representative trajectory of a vesicle decorated with 18-nt long DNA is plotted in Figure 2a, showing the autonomous movement for over 15 μm. To quantify the motility characteristics, we analyzed the moving trajectory to obtain velocity, travel distance, and mean squared displacement (Figures S11–S14 and S22). An average speed of ~0.5 nm/s is observed for this trajectory and also shown to be maintained throughout the trajectory, which indicates a highly consistent motion on the surface (Figure 2b and Figure S16). The ensemble statistics of the travel distance from all moving SVs are shown in Figure 2c. An average travel distance of 5 μm is observed with many trajectories showing as long as 20 μm (Figure S11). No significant displacements were observed in negative control experiments without nuclease or substrates (Figures S9–S11).

As natural cells only show chemotaxis in narrow concentration and response ranges,[31] the vesicle chasing behavior also relies heavily on environmental factors and motility characteristics. For example, a fast-moving SV with low processivity tend to show significant random hopping along its trajectory (Figure S15) rather than migrating on the surface continuously. To understand how experimental parameters affect motility, we measured vesicle velocity, travel time, and travel distance under different conditions (i.e., Mg^{2+} concentration, nuclease concentration, and DNA length), and extracted design principles for vesicle motility (Figure 2d–e and Figures S12–S14). The results suggest that a stable DNA-RNA duplex (i.e., longer DNA length, higher Mg^{2+} concentration, or lower enzyme concentration) increases SV's processivity on the surface while decreasing the moving velocity. Since the overall displacement is the product of travel time and speed, there exists a combination of parameters that achieve the highest processivity while maintaining relatively high speed (Figure 2e). For example, given the DNA length of 18-nt, the best condition for achieving processive motion may be chosen as 12 mM Mg^{2+} and 1 nM nuclease.

To develop directed motility mechanisms, we used signaling DNA molecules to modulate on/off SV motility. In a switchable RNA fuel, its 15-nt DNA-binding bases (Figure 3a, dark blue) are partially shielded by an intramolecular 10-nt RNA displacement strand (Figure 3a, gray). Various mechanisms may be used to activate the fuel.[17,32] In this work, the displacement strand is removed by a signaling 18-nt DNA strand through an 8-nt toehold (Figure 3a, red), followed by enzymatic cleavage and fuel activation. To prevent undesired leakage due to spontaneous strand displacement and activation by the DNA–vesicle (Figure 3a, green), we reduced the Mg^{2+} concentration to 3 mM. The speeds and trajectories are shown in Figure 3b,c for inactive and active fuels. Vesicles on active fuels exhibit similar migration behaviors as those in Figure 2 but have a significantly faster velocity and shorter total travel distance due to a lower Mg^{2+} concentration. In contrast, SVs on inactive fuels do not show any significant movement (Figure 3c). The velocity shown in Figure 3b with inactive fuels is due to random diffusion on the surface and localization errors from data analysis. The results indicate that the vesicle motility can be modulated by switchable RNA fuels whose activation characteristics may be exploited for implementing advanced vesicle behaviors.

We combined SV motility and switchable RNA fuels to program path tracking behaviors between different species of vesicles. The two SV types, lead and follow, are synthesized with 18-nt and 15-nt DNA strands, respectively (Figure 1b, red and green circles). To understand the expected chasing behaviors, we performed stochastic simulations where the vesicle dynamics are determined by the interplay between interaction forces from RNA fuels and thermal fluctuations (Figure 4a and Movie S3, also see Figures S21–S22). The simulation results are presented with dimensionless spatial coordinates (i.e., body length) and Fourier number, which is

$$Fo = \frac{Dt}{r^2} \quad (1)$$

where D is a diffusion coefficient, t is time, and r is the particle radius, i.e., body length. The availability of intact RNA fuels directly impacts the simulated motility. For the lead vesicle (Figure 4a, red circle), all RNA strands on the 2D plane are available as fuels (gray background) except for those that have been consumed before (visualized as a dark blue track). For the follow SV, the RNA strands are initially inactive; thus, its motility is only affected by thermal fluctuations, demonstrating Brownian dynamics in a confined area (Figure S23). When the vesicle (Figure 4a, green circle) starts from the same initial position after the lead vesicle movement, the activated RNA fuels exert additional binding forces and thus shift its dynamics from Brownian to self-avoiding with significantly increased motility and directionality on track (Figure S24). As a result of such chemotactic motility on activated fuels, the trajectories of the two vesicles are highly colocalized, suggesting significant path tracking behaviors in the simulation.

DOI: 10.1021/acs.nanolett.9b04428
Nano Lett. 2019, 19, 9138–9144

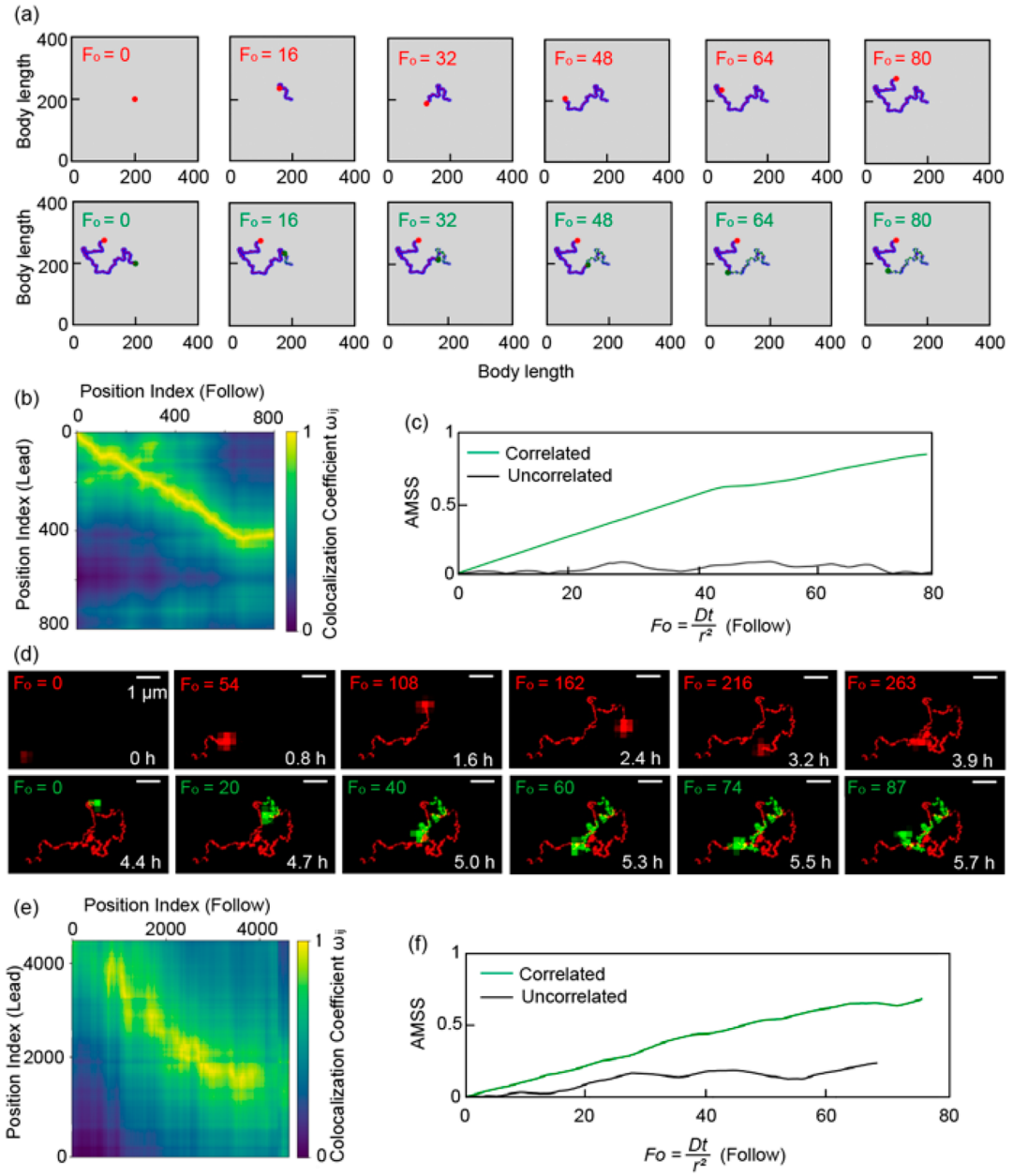

Figure 4. Programmed chemotactic vesicle migration. (a) Stochastic simulations of lead and follow SV dynamics. Representative images from the simulation are shown in dimensionless length (body length) and time (*Fo*). The red circle and the dark blue trajectory represent the lead vesicle and its consumed fuels (i.e., activated fuels for the follow SV), respectively. The green circle and trajectory denote the follow vesicle. (b) The colocalization coefficient, ω_{ij}, is plotted as a 2D heatmap along the two trajectories. High coefficient values along diagonal suggest a strong correlation between two trajectories. (c) AMSS plots of the simulation (green) and a negative control run (black) as a function of *Fo* show that the chasing behavior leads to AMSS rapidly approaching unity, while the AMSS of the negative control remains near 0. (d) Vesicle chasing experiment showing the trajectories of lead (red) and follow (green) SVs. The lead SV experiment is performed with 12 mM Mg^{2+}, while the follow SV's tracking is imaged with 3 mM Mg^{2+}. The enzyme concentration was kept at 1 nM throughout the experiment. (e) Colocalization coefficient of the trajectories of lead and follow SVs indicates that the two trajectories are closely positioned, as seen in the simulation. (f) AMSS analyses also show the close shape similarity and directionality, suggesting that chemotactic behavior via a path tracking mechanism is indeed observed between the lead and follow SVs.

To quantify such behaviors, we used the colocalization coefficient ω_{ij} and angular metric for shape similarity (AMSS; see supplementary text for details). Colocalization coefficient defined as

$$\omega_{ij} = \frac{\zeta_{max} - \zeta_{ij}}{\zeta_{max} + \zeta_{ij}} \quad (2)$$

measures the normalized spatial correlation. Here ζ_{ij} denotes the distance between any two points on the two trajectories, where i and j represent the position indices of lead and follow trajectories. When two positions on the trajectories are perfectly overlaid, the coefficient at this position will approach unity. We computed the distance ζ_{ij} of each position on the follow SV trajectory with all the positions on the lead SV trajectory. The coefficient from our simulations is plotted with respect to the position index on each trajectory and shown as a 2D heatmap. As seen in Figure 4b, near unity values align along the diagonal direction on the map, which indicates a high degree of pairwise

DOI: 10.1021/acs.nanolett.9b04428
Nano Lett. 2019, 19, 9138−9144

colocalization and correlation between the lead and follow trajectories. AMSS indicates the temporal correlation of two trajectories and is computed at each acquisition time point. For correlated trajectories, AMSS will rapidly increase to unity due to high shape similarity (i.e., directionality). We segmented the entire trajectory for both lead and follow vesicles into 120 s interval vectors and computed AMSS as time series. The results for the simulation data are shown in Figure 4c as a function of Fourier number. Compared to the uncorrelated negative control (Figure S23), AMSS show trends consistent with strong correlations between the two trajectories.

To demonstrate SV chasing experimentally, we performed sequential experiments with lead and follow vesicles (Figure 4d and Movie S4). The lead vesicle shows similar motion dynamics as the vesicle on straight fuels in Figure 2 but has a shorter travel distance and higher average velocity, e.g., ∼1 nm/s (Figure S17). This observation is consistent with our design as part of the 18-nt lead fuel is shielded and must go through strand displacement before nuclease consumption. After lead vesicle migration, follow vesicles were introduced and randomly searched for activated fuels. If a follow vesicle intersected the lead SV's path as its initial position, it started to follow the track. Note that, for follow vesicles that did not intersect with lead vesicle paths, no significant movements or speed were observed as all RNA fuels were inactive for follow SV migration as seen in Figure 3c. Unlike the simulations where the follow vesicle always starts from the same origin as the lead vesicle, the follow SV in tracking experiments starts randomly on the lead SV trajectory and can move toward either direction. Once it migrates in a particular direction, it will continue to trail the path because its motion outside the path will be suppressed. The trajectories in Figure 4d show that the follow vesicle moved in the opposite direction on the lead vesicle path, and the colocalization coefficient graph in Figure 4e is thus plotted with a reversed position index to reflect the directionality. Both colocalization coefficient and AMSS analyses demonstrate a strong correlation between the lead and follow trajectories (Figure 4f), consistent with those shown in simulations. The negative control of uncorrelated SVs does not show any significant trajectory colocalization for the follow vesicle (Figure S19).

Further analysis confirms the follow vesicle's designed chemokinetic behaviors. In natural chemotaxis, neutrophils, for example, chemokinetic motility plays a critical role in chasing and eliminating bacteria. In the path tracking experiment, the follow vesicle migrated with significantly greater velocity (increased by ∼50%) than the lead vesicle (Figure S18). This results from our DNA motif design as the follow vesicle has a shorter walker length (15-nt) than the lead vesicle (18-nt), consistent with Figure 2e. Additional data for chasing between lead and follow vesicles is presented in Figure S20 and Movie S5. To the best of our knowledge, this is the first demonstration of DNA programmed coordination between two migrating vesicles.

In conclusion, we have demonstrated SVs with DNA-driven motility and adaptability. The vesicles explore their surroundings on the surface and respond to biochemical cues to execute programmed behaviors. One major challenge in realizing surface chemotaxis in synthetic cellular systems is the lack of compatible molecular components capable of chemical communication, signal modulation, and mechanical translocation. In this work, we used DNA programmed molecular switches to achieve these functions. Our tracking experiments suggest that, with chemotactic and chemokinetic motility, predator−prey relations such as pursuit predation will be possible in artificial cellular systems. In our design, biochemical signals from the lead vesicle are implemented as the half-burnt fuels along the trajectory, which provides directionality and path tracking ability for the follow vesicle. With enhanced velocity, the path-tracking follow vesicle shows both directed motility and chemokinesis. In natural chemotaxis, however, diffusing biochemical signals (e.g., proteins and ATP) form gradients and direct cellular motions. This may inspire the development of new molecular mechanisms for responding to biochemical gradients and achieving complete synthetic chemotaxis.

Further, biomimetic chemical communications will also be possible from bottom-up using engineered DNA molecules. In nature, cell-to-cell communications via chemical signals enable coordinated, collective behaviors in cell colonies[33] and multicellular organisms.[34] With the rapid development of various DNA nanotechnology tools, we envision that dynamic synthetic protocells with sensors and intelligence may be constructed, demonstrating more complex functions such as programmed morphogenesis and cooperative motion. Such self-organizing artificial systems may become a model system for abiogenesis and soft matter physics, and could lead to novel applications in diverse engineering disciplines.

Materials and Methods. *Materials.* All DNA and RNA sequences were custom-synthesized by Integrated DNA Technologies. The sequence information is listed in Table S1. Phosphate buffered saline (PBS) containing 137 mM NaCl, 2.7 mM KCl, 1.8 mM KH_2PO_4, 10 mM Na_2HPO_4, and sodium-tris-ethylenediaminetetraacetic acid (EDTA) buffer (pH 8.0; 20 mM tris-HCl, 0.5 mM EDTA, 100 mM NaCl) was prepared in deionized water (18 MΩ). All lipids were purchased from Avanti Polar Lipids. RNase H (New England Biolabs), which cleaves substrates longer than 7-nt, was exploited in our fuel design.[35] Other nucleases (e.g., Exo III and lambda exonuclease) may also be used for vesicle migration. All reagents were purchased from Click Chemistry Tools unless noted otherwise.

Sample Preparation. DNA decorated vesicles and RNA-modified fuel surfaces were prepared separately before the experiments. Azide−DNA was synthesized by conjugating amine−DNA and azide-$(polyethylene\ glycol)_4$-*N*-hydroxysuccinimide (azide-$(PEG)_4$-NHS). The DNA−lipid conjugate was synthesized using azide−DNA mixed with 1,2-distearoyl-*sn*-glycero-3-phosphoethanolamine-*N*-[dibenzocyclooctyl(PEG)-2000] (DSPE-PEG(2000)-DBCO) at a 1:5 ratio by click chemistry. DNA decorated vesicles were prepared with a dehydration−rehydration method. Lipids used in vesicle assembly include 1,2-dimyristoyl-*sn*-glycero-3-phosphoethanolamine (14:0 PE), 1,2-dipalmitoyl-*sn*-glycero-3-phosphocholine (16:0 PC), 1,2-dimyristoyl-*sn*-glycero-3-phosphoethanolamine-*N*-(lissamine rhodamine B sufonyl) (ammonium salt),or 14:0 Liss Rhod PE. The lipid mixture (14:0 PE, 16:0 PC, 14:0 Liss Rhod PE) dispersed in chloroform was incubated with the synthesized DNA−lipid conjugate in PBS at a molar ratio of 50:50:1:1, respectively. The mixed solution was dried in a vacuum chamber to form lipid bilayers and rehydrated with 1 mL of PBS buffer and heated to 90 °C. The mixture was stirred at 500 rpm for an hour, forming vesicles.

DBCO-RNA was synthesized by conjugating amine-modified RNA with DBCO-NHS. Glass coverslips were etched in Piranha solution (3:1 v/v sulfuric acid/hydrogen peroxide) for 30 min and washed with sufficient deionized (DI) water and ethanol. Silanization was performed with approximately 100 μL 5% (v/v) 3-azidopropyltriethoxysilane in dimethylformamide (DMF) on

DOI: 10.1021/acs.nanolett.9b04428
Nano Lett. 2019, 19, 9138−9144

a coverslip and another coverslip on top forming a sandwich structure incubated overnight. After that, both coverslips were washed with ethanol. Approximately, 100 μL of 50 μM DBCO-RNA was added on the azide-modified surface with another surface on top. The sandwiched coverslips were incubated overnight and washed with DI water. The fuel surface was stored at −20 °C.

Experimental Procedure. A microfluidic imaging channel was assembled using the RNA fuel decorated coverslip and a quartz slide. The fuel surface was passivated with 30 μL of 10 mM DBCO-$(PEG)_4$-NHS flown into the channel and incubated for 30 min. Then, 30 μL of 15% amine-$(PEG)_4$-NHS was introduced into the channel and incubated for another 30 min. After the incubation, sufficient PBS solution was supplied into the channel to remove unbound passivation reagents. Lead vesicle solution ($\sim 10^{12}$/mL) was introduced into the imaging channel by a syringe and incubated for 5 min for vesicles to bind to the surface. Approximately, 500 μL of PBS buffer was flown into the channel to wash away unbound vesicles. Then, 50 μL of 1× nuclease buffer adjusted to a final concentration of 12 mM $MgCl_2$ was supplied to the channel followed by the introduction of the RNase H (New England Biolabs) solution at 1 nM. The lead vesicle dynamics was imaged for 8 h. After the imaging, approximately 1 mL of DI water was supplied into the channel to wash away the lead vesicles. The follow vesicles ($\sim 10^{11}$/mL) and nuclease solution (final concentration of 1 nM) were then introduced into the imaging channel. The follow vesicle motion was also imaged for 8 h.

Imaging System. A custom-built TIRF microscope (Zeiss Axio Observer D1) was used for imaging vesicle migration. The excitation light from a 561 nm diode laser (Laserglow) was introduced to the sample through an oil-immersion 63× objective lens at approximately 10 mW. The collected emission light from the sample was imaged with an Andor iXon3 electron-multiplying charge-coupled device (EMCCD) camera. The imaging was performed at room temperature with an exposure time of 200 ms and an interval of 1 s.

Analysis of the Path Tracking Behavior. The data of path tracking behavior was analyzed based on spatial and temporal correlations. First, the colocalization coefficient ω_{ij} is used to measure whether the trajectories of lead and follow vesicles are matched spatially. The lead trajectory is represented by a series of coordinates (lx_i, ly_i), where $i = 0, 1, 2, ..., m$. The follow trajectory is represented by a series of coordinates (fx_j, fy_j), where $j = 0, 1, 2, ..., n$. ζ_{ij} is the Euclidean distance between two points and calculated as

$$\zeta_{ij} = \sqrt{(lx_i - fx_j)^2 + (ly_i - fy_j)^2} \tag{3}$$

This forms a 2D matrix of the Euclidean distances between any two points on the lead and follow trajectories. ζ_{max} can be identified from the 2D matrix. The colocalization coefficient ω_{ij} is then obtained as in eq 2, which is also a 2D matrix, and a heatmap can be plotted based on ω_{ij}. This coefficient ranges from 0 to 1. If two points on the trajectories are colocalized perfectly, $\zeta_{ij} = 0$ and $\omega_{ij} = 1$. When two points are not colocalized, the Euclidean distance $\zeta_{ij} > 0$ and $\omega_{ij} < 1$. When the distance between the two points is further, the coefficient will be smaller. When the trajectories of the lead and follow vesicles are overlaid, a distinct line of $\omega_{ij} \approx 1$ will be formed along the diagonal, as shown in the heatmaps in Figure 4 and Figure S20. When the trajectories are not correlated, no line will be formed in the heatmap as shown in Figures S19 and S23.

The AMSS[36] is used to measure the shape similarity between two trajectories regardless of their length scale differences. This angular metric is defined based on the angle between the two vesicles' moving vectors.

$$\begin{aligned} &\mathrm{AMSS}\ (R_m, S_n) \\ &= \max\begin{cases} \mathrm{AMSS}\ (R_{m-1}, S_{n-1}) + 2sim\ (r_n, s_n) \\ \mathrm{AMSS}\ (R_{m-2}, S_{n-1}) + 2sim\ (r_{m-1}, s_n) + sim\ (r_m, s_n) \\ \mathrm{AMSS}\ (R_{m-1}, S_{n-2}) + 2sim\ (r_m, s_{n-1}) + sim\ (r_m, s_n) \end{cases} \end{aligned} \tag{4}$$

where r_m and s_n represent moving vectors at step m and step n on the two trajectories. The similarity between the moving vectors is defined as

$$sim\ (r_m, s_n) = \frac{\overrightarrow{r_m} \cdot \overrightarrow{s_n}}{\|\overrightarrow{r_m}\| \cdot \|\overrightarrow{s_n}\|} \tag{5}$$

which ranges from 0 to 1. The AMSS is plotted as a function of time. If the moving vectors are closely aligned during the entire period of time, $sim = 1$, and the AMSS increases rapidly. In contrast, if the two vectors move toward the opposite direction, $sim = -1$, and the AMSS decreases with time. In our analysis, the AMSS graphs are plotted with absolute values regardless of moving directions and normalized with theoretical maximum assuming the perfect alignment of trajectories (i.e., $0 \le \mathrm{AMSS} \le 1$), as shown in Figure 4f. This serves as a useful method to measure the similarity between the lead and follow vesicles' trajectories temporally.

To generalize temporal behaviors, we used Fourier number Fo, defined as in eq 1. The diffusion coefficient D was calculated based on the MSD measurements (Figure S22) using the following expression:[37]

$$D = \lim_{t \to \infty} \frac{\langle [\Delta R(t)]^2 \rangle}{2dt} \tag{6}$$

where d is the dimension, and ΔR is the displacement of the center-of-mass after time t. The calculated diffusion coefficient in our experiment is roughly $D \approx 187$ nm^2/s.

Stochastic Simulations. A stochastic simulation model was derived from the Langevin equation,[38] and the motion is governed by

$$\frac{\Delta \boldsymbol{r}}{R} = \frac{\boldsymbol{F}R}{k_B T} Fo + \sqrt{4Fo}\,\boldsymbol{\xi} \tag{7}$$

where $\boldsymbol{F}$ is the fuel binding force, k_B is the Boltzmann constant, T indicates temperature, R is the vesicle radius, Fo is Fourier number, and $\boldsymbol{\xi}$ is the direction vector of random diffusion. The simulation of path tracking behavior was performed using the above equation. The lead vesicle started from the middle of the simulation domain and migrated on the fuel surface. The explored fuels were recorded as available for the follow vesicle. The follow vesicle then started from the same starting point and can only move on the activated fuels, thus tracking the trajectory of the lead vesicle closely.

■ ASSOCIATED CONTENT

Supporting Information

The Supporting Information is available free of charge on the ACS Publications website at DOI: 10.1021/acs.nanolett.9b04428.

Sequence design, preparation, and characterization of vesicles and surfaces, experimental setup and procedures,

DOI: 10.1021/acs.nanolett.9b04428
Nano Lett. 2019, 19, 9138−9144

detailed analysis, simulations, control experiments, and figures (PDF)
Movie S1 (AVI)
Movie S2 (AVI)
Movie S3 (AVI)
Movie S4 (AVI)
Movie S5 (AVI)

AUTHOR INFORMATION

Corresponding Author

*E-mail: jchoi@purdue.edu.

ORCID

Jong Hyun Choi: 0000-0002-0507-3052

Author Contributions

†J.P. and Y.D. contributed equally to this work

Notes

The authors declare no competing financial interest.

ACKNOWLEDGMENTS

This work was funded by the U.S. Office of Naval Research (N00014-15-1-2707). J.H.C. also acknowledges partial support from the U.S. National Science Foundation (1710344).

REFERENCES

(1) Alberts, B. et al. *Mol. Biol. Cell.*, 6th ed; Garland Science: New York, 2014.
(2) Parent, C. A. Making all the right moves: chemotaxis in neutrophils and Dictyostelium. *Curr. Opin. Cell Biol.* **2004**, *16*, 4−13.
(3) Keller, H.; Wissler, J.; Hess, M.; Cottier, H. Distinct chemokinetic and chemotactic responses in neutrophil granulocytes. *Eur. J. Immunol.* **1978**, *8*, 1−7.
(4) Kurihara, K.; et al. A Recursive Vesicle-based Model Protocell with a Primitive Model Cell Cycle. *Nat. Commun.* **2015**, *6*, 8352.
(5) Stewart, M. P.; et al. In Vitro and Ex Vivo Strategies for Intracellular Delivery. *Nature* **2016**, *538*, 183−192.
(6) Elani, Y.; Law, R. V.; Ces, O. Vesicle-based Artificial Cells as Chemical Microreactors with Spatially Segregated Reaction Pathways. *Nat. Commun.* **2014**, *5*, 5305.
(7) Adamala, K. P.; Martin-Alarcon, D. A.; Guthrie-Honea, K. R.; Boyden, E. S. Engineering genetic circuit interactions within and between synthetic minimal cells. *Nat. Chem.* **2017**, *9*, 431.
(8) Göpfrich, K.; Platzman, I.; Spatz, J. P. Mastering Complexity: Towards Bottom-up Construction of Multifunctional Eukaryotic Synthetic Cells. *Trends Biotechnol.* **2018**, *36*, 938−951.
(9) Joseph, A.; et al. Chemotactic Synthetic Vesicles: Design and Applications in Blood-Brain Barrier Crossing. *Science Advances* **2017**, *3*, No. e1700362.
(10) Seeman, N. C.; Sleiman, H. F. DNA Nanotechnology. *Nature Reviews Materials* **2018**, *3*, 17068.
(11) Rothemund, P. W. K. Folding DNA to Create Nanoscale Shapes and Patterns. *Nature* **2006**, *440*, 297−302.
(12) Ke, Y.; Ong, L. L.; Shih, W. M.; Yin, P. Three-Dimensional Structures Self-Assembled from DNA Bricks. *Science* **2012**, *338*, 1177−1183.
(13) Gold, L.; et al. Aptamer-Based Multiplexed Proteomic Technology for Biomarker Discovery. *PLoS One* **2010**, *5*, No. e15004.
(14) Thubagere, A. J.; et al. A Cargo-Sorting DNA Robot. *Science* **2017**, *357*, No. eaan6558.
(15) Yurke, B.; Turberfield, A. J.; Mills, A. P., Jr.; Simmel, F. C.; Neumann, J. L. A DNA-Fuelled Molecular Machine Made of DNA. *Nature* **2000**, *406*, 605−608.
(16) Cha, T.-G.; et al. A synthetic DNA motor that transports nanoparticles along carbon nanotubes. *Nat. Nanotechnol.* **2014**, *9*, 39−43.
(17) Green, A. A.; et al. Complex cellular logic computation using ribocomputing devices. *Nature* **2017**, *548*, 117−121.
(18) Seelig, G.; Soloveichik, D.; Zhang, D. Y.; Winfree, E. Enzyme-Free Nucleic Acid Logic Circuits. *Science* **2006**, *314*, 1585−1588.
(19) Chen, Y.-J.; Groves, B.; Muscat, R. A.; Seelig, G. DNA Nanotechnology from the Test Tube to the Cell. *Nat. Nanotechnol.* **2015**, *10*, 748−760.
(20) Packer, H. L.; Armitage, J. P. The Chemokinetic and Chemotactic Behavior of Rhodobacter sphaeroides: Two Independent Responses. *J. Bacteriol.* **1994**, *176*, 206−212.
(21) Lund, K.; et al. Molecular Robots Guided by Prescriptive Landscapes. *Nature* **2010**, *465*, 206−210.
(22) Gu, H.; Chao, J.; Xiao, S. J.; Seeman, N. C. A Proximity-Based Programmable DNA Nanoscale Assembly Line. *Nature* **2010**, *465*, 202−205.
(23) Yehl, K.; et al. High-Speed DNA-Based Rolling Motors Powered by RNase H. *Nat. Nanotechnol.* **2016**, *11*, 184−190.
(24) Qu, X.; et al. An Exonuclease III-Powered, On-Particle Stochastic DNA Walker. *Angew. Chem., Int. Ed.* **2017**, *56*, 1855−1858.
(25) Wickham, S. F. J.; et al. Direct Observation of Stepwise Movement of a Synthetic Molecular Transporter. *Nat. Nanotechnol.* **2011**, *6*, 166−169.
(26) Cha, T. G.; et al. Design Principles of DNA Enzyme-Based Walkers: Translocation Kinetics and Photoregulation. *J. Am. Chem. Soc.* **2015**, *137*, 9429−9437.
(27) Kopperger, E.; Pirzer, T.; Simmel, F. C. Diffusive Transport of Molecular Cargo Tethered to a DNA Origami Platform. *Nano Lett.* **2015**, *15*, 2693−2699.
(28) Li, J.; et al. Exploring the Speed Limit of Toehold Exchange with a Cartwheeling DNA Acrobat. *Nat. Nanotechnol.* **2018**, *13*, 723−729.
(29) Pan, J.; Li, F.; Cha, T.-G.; Chen, H.; Choi, J. H. Recent progress on DNA based walkers. *Curr. Opin. Biotechnol.* **2015**, *34*, 56−64.
(30) Pan, J.; et al. Visible/Near-Infrared Subdiffraction Imaging Reveals the Stochastic Nature of DNA Walkers. *Science Advances* **2017**, *3*, No. e1601600.
(31) Jeon, N. L.; Baskaran, H.; Dertinger, S. K. W.; Whitesides, G. M.; Van De Water, L.; Toner, M. Neutrophil chemotaxis in linear and complex gradients of interleukin-8 formed in a microfabricated device. *Nat. Biotechnol.* **2002**, *20*, 826.
(32) Feagin, T. A.; Maganzini, N.; Soh, H. T. Strategies for Creating Structure-Switching Aptamers. *ACS Sensors* **2018**, *3*, 1611−1615.
(33) Miller, M. B.; Bassler, B. L. Quorum Sensing in Bacteria. *Annu. Rev. Microbiol.* **2001**, *55*, 165−199.
(34) Mayor, R.; Etienne-Manneville, S. The Front and Rear of Collective Cell Migration. *Nat. Rev. Mol. Cell Biol.* **2016**, *17*, 97−109.
(35) Figiel, M.; Krepl, M.; Poznanski, J.; Gołab, A.; Sponer, J.; Nowotny, M. Coordination between the polymerase and RNase H activity of HIV-1 reverse transcriptase. *Nucleic Acids Res.* **2017**, *45*, 3341−3352.
(36) Nakamura, T.; Taki, K.; Nomiya, H.; Seki, K.; Uehara, K. A shape-based similarity measure for time series data with ensemble learning. *Pattern Analysis and Applications* **2013**, *16*, 535−548.
(37) Leegwater, J. A. Diffusion of a self-avoiding polymer. *Phys. Rev. E: Stat. Phys., Plasmas, Fluids, Relat. Interdiscip. Top.* **1995**, *52*, 2801.
(38) Ermak, D. L.; McCammon, J. A. Brownian dynamics with hydrodynamic interactions. *J. Chem. Phys.* **1978**, *69*, 1352−1360.

DOI: 10.1021/acs.nanolett.9b04428
Nano Lett. 2019, 19, 9138−9144